Numerical Investigation of Flow over a Canard Controlled Missile Configuration in Subsonic and Transonic Flow Regimes

Harish M [1], Keerthi Varman N [2], Muthu Kumar R[3]. Kavin R [4], Renuga R [5]
[1] *Assistant Professor, Department of Aeronautical Engineering,*
[2,3,4,5] *Student, Department of Aeronautical Engineering,*
Hindusthan Institute of Technology, Coimbatore, Tamilnadu, India.

Abstract

The transonic aerodynamics of a missile body is critical, which dictates the structural design aspect and controllability of the vehicle. ANSYS-FLUENT has been used to investigate the aerodynamic characteristics over a Canard controlled missile configuration for subsonic and transonic Mach numbers ranging from 0.6 to 2. The co-efficient of pressure, shock location, flow separation and reattachment regions have been extracted.

Keywords – *Missiles, Canard, Fins, Transonic Aerodynamics*

I. INTRODUCTION TO MISSILES

A missile is a self-propelled precision guidance system. An object which is forcibly propelled at a target, either manually or from a mechanical weapon. A canard is an aeronautical arrangement where a small forewing or fore plane is placed forward of the tail wing of an aircraft. The term canard may be used to describe the aircraft itself, the wing configuration or the fore plane. Rather than using the conventional configuration, an aircraft designer may adopt the canard configuration in order to reduce the main wing loading, to better control the main wing airflow, to increase the aircraft's maneuverability especially at high angle of attack or during a stall, to have better longitudinal equilibrium, static and dynamic stability characteristics and to reduce profile drag.

A. B. Blair, Jr., Jerry M. Allen, and Gloria Hernandez [1] conducted an experimental wind-tunnel investigation over a canard-controlled missile configuration at Mach numbers ranging from 1.60 to 3.50. The longitudinal and lateral-directional aerodynamic characteristics of a circular, cruciform, canard controlled missile with variations in tail-fin span were obtained. Canard roll control at low angles of attack is feasible on tail- fin configuration with tail-to-canard span ratios of less than or equal to 0.75.

Curtis P. Mracek and D. Brett Ridgley [2] conducted an experimental investigation on dual controlled missiles on optimal control problem. The dual controlled missiles responded with increased speed and has robustness characteristics when compared with a single tail or canard controlled missiles. But designing the canard and fin controls together linearly caused many aerodynamics problems due to the downwash of the canard on the fins.

Hong Chuan Wee [3] conducted a wind tunnel test on canard missile configuration for Mach numbers of 0.2, 0.8 and 1.2. The Computational Fluid Dynamics code, ANSYS-CFX have been used to predict the static aerodynamic characteristics of a canard-wing missile configuration. The ANSYS-CFX results shown good agreement for CN, CM, and CL but less agreement for CA when compared to the experimental results due to the turbulence models used.

James Despirito, Milton E. Vaughn Jr. & W. David [4] conducted an experimental investigation on canard missile with planar and grid fin configurations and validated the canard control effectiveness. Flow visualizations showed that the canard down wash produced a low-pressure region on the starboard side of the missile that produced a large induced side force. The canard trailing vortices interacted with the tail fins until $\alpha > 8°$, producing a pressure differential on the leeward tail fin, leading to the adverse induced roll effects.

Scott M. Murman S [5] conducted an experimental investigation on canard missile with a spinning tail to determine their behaviours. Time-dependent, relative-motion simulations were performed using an inviscid Cartesian-grid-based method at three angles of attack. The results indicate that the choice of a static, forced-spin, or free-to-spin analysis cannot in general be made a priority. Further, the behaviour of the dynamic tail section is likely multi-valued, and hence the state for any configuration is dependent upon the function of the missile.

II. CONFIGURATION STUDIED

The following section outlines the geometrical features of various missile configurations used for CFD simulation. Configuration 1shown in figure 1

represents the missile with wedge canard and clipped delta fin. Configuration 2 shown in figure 2 represents the missile with trapezoidal canard and clipped delta fin.

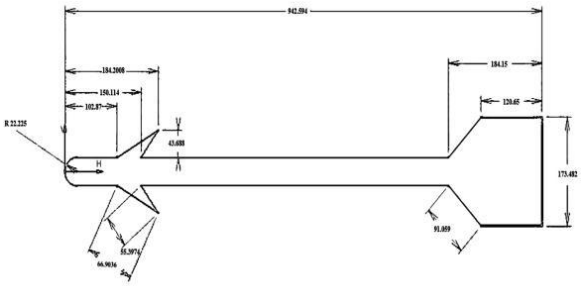

Figure 1 – Configuration 1 Geometric Details (All Dimensions are in mm)

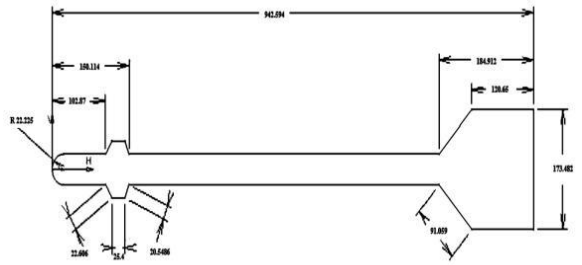

Figure 2 – Configuration 1 Geometric Details (All Dimensions are in mm)

III. GRID GENERATION AND CFD SOLVER

CFD is an integral part of the design process. In this paper, multi-block structured grids are generated over the 2D axi-symmetric canard configurations using *GRIDGEN* tool. The primary parameter which determines the minimum number of grid points is the boundary layer thickness. For accurate simulation of separation and shock location, the first grid point off the surface should lie within the sub layer where the velocity varies linearly with distance from the surface. To capture boundary and shock boundary layer interaction finer grids are used near the body. The grid is generated over only one half of the model which is Axi-symmetric. Three types of boundary conditions are used for the computation of flow field, i.e., wall, pressure far field and symmetry conditions. The grid distribution and boundary conditions over canard controlled missile configuration is shown in figure 3. CFD simulation have been carried out over 2-D Axis-symmetric canard missile configuration using Spalart - Allmaras (1 EQN) Viscous model for Mach numbers ranging from 0.6 to 2. All the CFD simulations have been carried out using *ANSYS-FLUENT*.

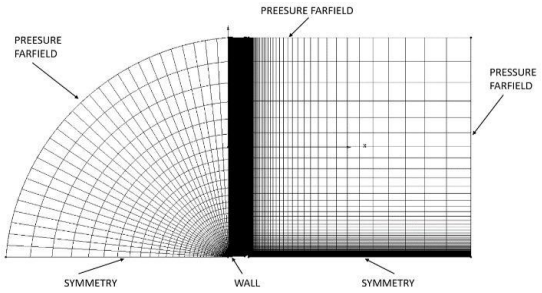

Figure 3 - Grid distribution and boundary conditions over canard controlled missile configuration

IV. GRID INDEPENDENCE STUDY AND CFD SIMULATION

The grid independence study has been carried out over the canard configurations with three different mesh sizes. The grid distribution and specifications are shown in figure 4 to 6. Figure 7 shows the coefficient of pressure, Cp distribution over canard configurations for the three meshes namely mesh 10K, mesh 20K, and mesh 30K. It can be seen from the figure that, for further increase in the number of meshes, no considerable rise in coefficient of pressure around the missile body is observed. Hence the optimum mesh size has been taken as mesh 20K.

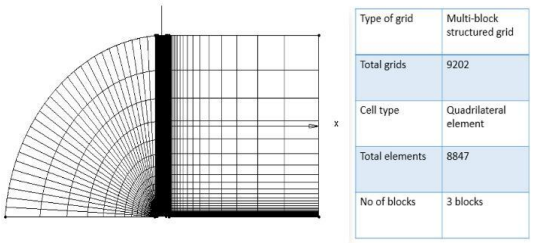

Type of grid	Multi-block structured grid
Total grids	9202
Cell type	Quadrilateral element
Total elements	8847
No of blocks	3 blocks

Figure 4 – Grid distribution of mesh size 10K

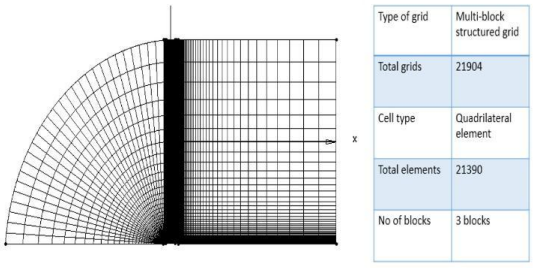

Type of grid	Multi-block structured grid
Total grids	21904
Cell type	Quadrilateral element
Total elements	21390
No of blocks	3 blocks

Figure 5 – Grid distribution of mesh size 20K

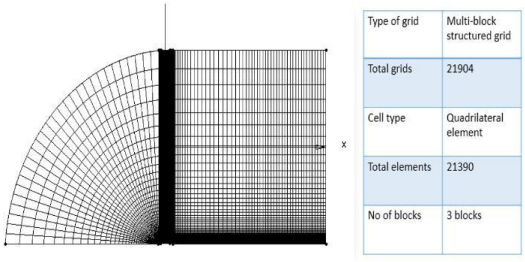

Type of grid	Multi-block structured grid
Total grids	21904
Cell type	Quadrilateral element
Total elements	21390
No of blocks	3 blocks

Figure 6 – Grid distribution of mesh size 30K

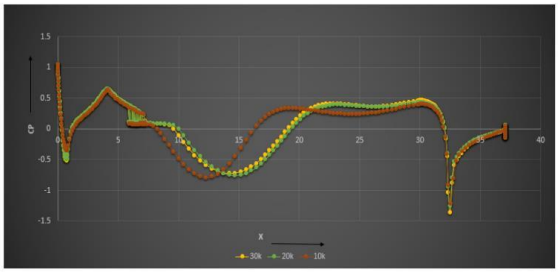

Figure 7 – The Co-efficient of pressure distribution over canard configuration for three different meshes at M 0.6

V. RESULTS AND DISCUSSION

CFD simulations have been carried out over both the missile configurations for Mach numbers 0.6, 0.8, 0.9, 1.1, 1.3 and 2. Figures 8 shows the Coefficient of pressure, Cp distribution over the configuration 1 for the Mach numbers of 0.6 to 2 respectively. The Cp plot reveals that the initial peak in Cp is due to the stagnation point (first contact of the flow over the nose) and then Cp decreases as the flow expands over the body. There is a Cp jump i.e., increase in the pressure over the canard wing for all the Mach numbers, which is due to the formation of normal shock and then Cp decreases due to the occurrence of expansion fan at the wing tip. The Cp then falls and rises gradually soon after the wing due to the wake region and remains constant over the missile body. There is an another jump in Cp seen over the fin due to the formation of normal shock and then the Cp decreases due to the occurrence of expansion fan at the fin tip. The Cp then gradually falls and rises again due to the wake region seen soon after the fin and remains constant thereafter. The Cp plot clearly shows that the transonic shock which is seen near the canard wing moves further downstream with increase in freestream Mach number.

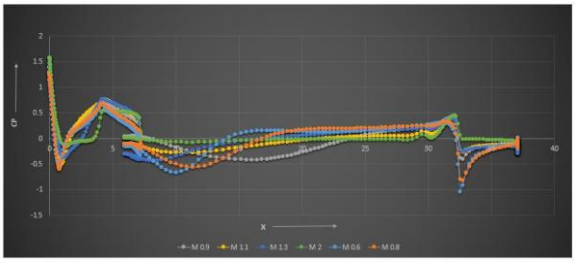

Figure 8 - Coefficient of pressure, Cp distribution over the configuration 1 for all the Mach numbers

Figures 9 shows the Skin-friction coefficient, Cf distribution over the configuration 1 for the Mach numbers of 0.6 to 2. The plot reveals that the point at which Cf is negative indicates the flow separation and the point at which Cf is positive indicates the reattachment of the flow. Flow separation is observed soon after the wing for all Mach numbers, where the Cf is negative. This flow separation is confined to a short distance and reattaches over the mid body and then remains constant. Another negative value of Cf is observed soon after the fin for all Mach numbers, indicating another flow separation region. This flow separation is small and gets reattached immediately downstream the fin.

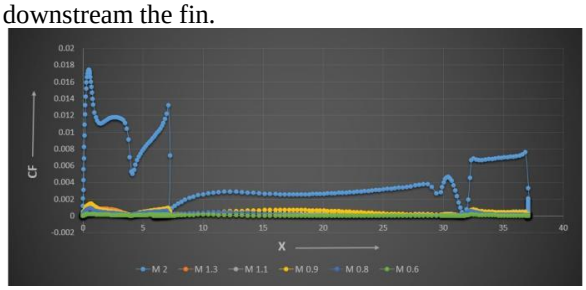

Figure 9 - Skin-friction coefficient, Cf distribution over the configuration 1 for all the Mach numbers

Figures 10 shows the contours of Mach number over the canard configurations for the Mach numbers of 0.6 to 2. The Mach contour plot reveals that, the supersonic region seen near the wing and the fin is due to the occurrence of expansion fans, increases with increase in free stream Mach number and the terminal shock moves downstream. It can be seen from the figure that the movement of the terminal shock is a nonlinear function of Mach number (i.e. for an equal interval of Mach number increase, the increase in shock movement is larger), which is also observed from pressure and density contour plots from figures 11 and figures 12. The location of shock waves over the canard configuration is shown in figures 15.

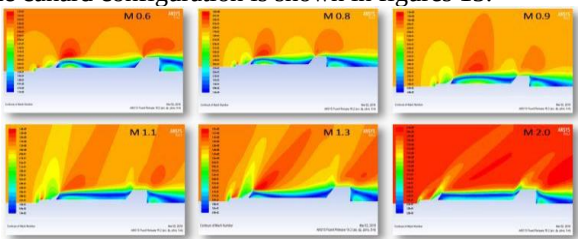

Figure 10 - Mach contour comparison of configuration 1 for all Mach numbers

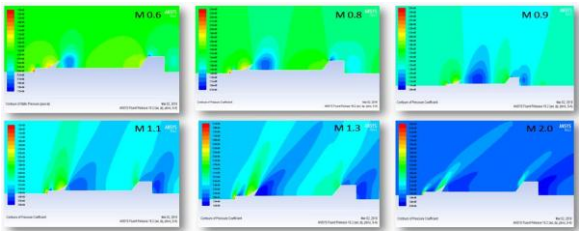

Figure 11 - Pressure contour comparison of configuration 1 for all Mach numbers

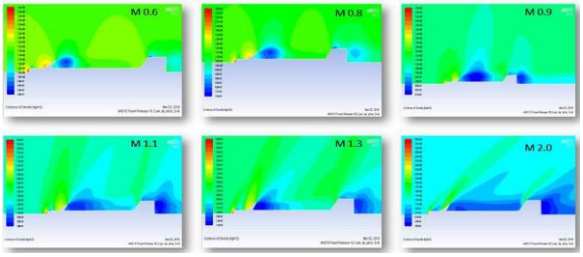

Figure 12 - Density contour comparison of configuration 1 for all Mach numbers

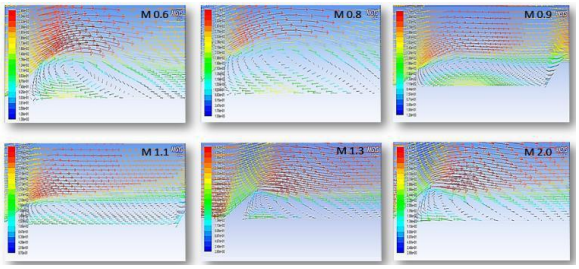

Figure 13 - Velocity vectors at wings of configuration 1 for all Mach numbers

Figures 13 and figures 14 shows the velocity vector plots over the canard configurations at the wings and fins for the Mach numbers of 0.6 to 2 respectively. The vector plot reveals that flow separation and reattachment is observed for all the Mach numbers. The flow gets separated near the wing tip and then later reattaches over the missile centre body.

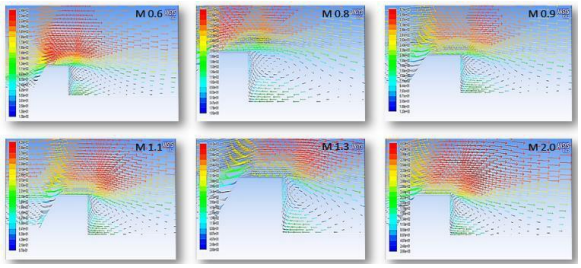

Figure 14 - Velocity vectors at fins of configuration 1 for all Mach numbers

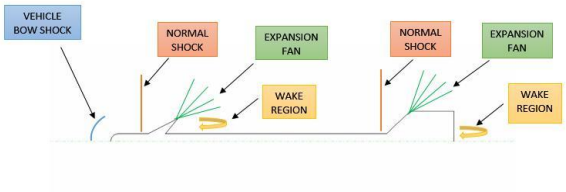

Figure 15 - The location of shock waves over configuration 1

The region in between the point of separation and point of reattachment is called as the wake region or recirculation region. Similarly, there is a small wake region soon after the fin is observed for all the Mach numbers. The wake region increases with increase in freestream Mach numbers from 0.6 to 1.1, and then it decreases for Mach numbers 1.3 and 2 for all the configurations.

Figures 16 shows the Coefficient of pressure, Cp distribution over the configuration 2 for the Mach numbers of 0.6 to 2 respectively. The Cp plot reveals that the initial peak in Cp is due to the stagnation point (first contact of the flow over the nose) and then Cp decreases as the flow expands over the body. There is a Cp jump i.e., increase in the pressure over the canard wing for all the Mach numbers, which is due to the formation of normal shock and then Cp decreases due to the occurrence of expansion fan at the wing tip.

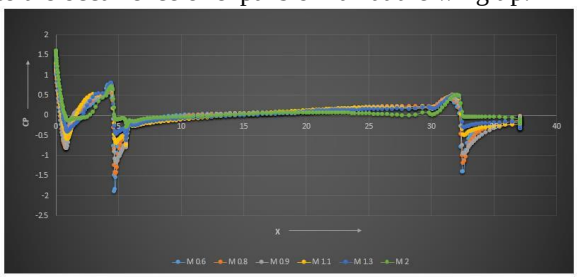

Figure 16 - Coefficient of pressure, Cp distribution over the configuration 2 for all the Mach numbers

The Cp then falls and rises gradually soon after the wing due to the wake region and remains constant over the missile body. There is an another jump in Cp seen over the fin due to the formation of normal shock and then the Cp decreases due to the occurrence of expansion fan at the fin tip. The Cp then gradually falls and rises again due to the wake region seen soon after the fin and remains constant thereafter. The Cp plot clearly shows that the transonic shock which is seen near the canard wing moves further downstream with increase in freestream Mach number.

The Figure 17 shows the Skin-friction coefficient, Cf distribution over the configuration 1 for the Mach numbers of 0.6 to 2. The plot reveals that the point at which Cf is negative indicates the flow separation and the point at which Cf is positive indicates the reattachment of the flow. Flow separation is observed soon after the wing for all Mach numbers, where the Cf is negative. This flow separation is confined to a short distance and reattaches over the mid body and then remains constant. Another negative value of Cf is observed soon after the fin for all Mach numbers, indicating another flow separation region. This flow separation is small and gets reattached immediately downstream the fin.

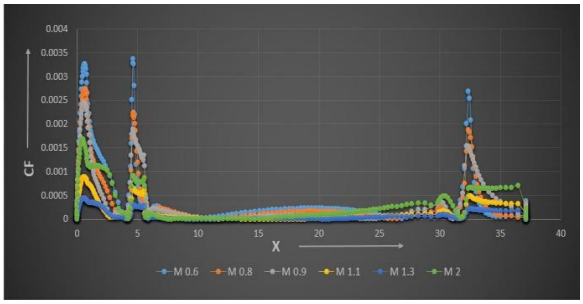

Figure 17 - Skin-friction coefficient, Cf distribution over the configuration 2 for all the Mach numbers

Figure 18 shows the contours of Mach number over the canard configurations for the Mach numbers of 0.6 to 2. The Mach contour plot reveals that, the supersonic region seen near the wing and the fin is due to the occurrence of expansion fans,

Increases with increase in free stream Mach number and the terminal shock moves downstream.

It can be seen from the figure that the movement of the terminal shock is a nonlinear function of Mach number (i.e. for an equal interval of Mach number increase, the increase in shock movement is larger), which is also observed from pressure and density contour plots from figure 19 and figure 20. The location of shock waves over the canard configuration is shown in figure 23.

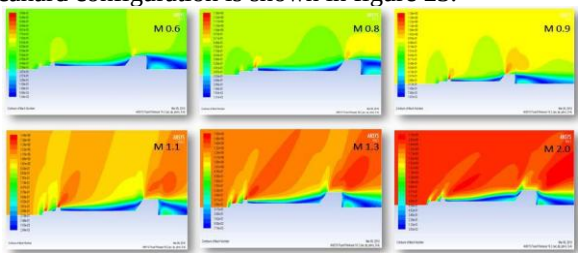

Figure 18 - Mach contour comparison of configuration2 for all Mach numbers

Figures 21 and 22 shows the velocity vector plots over the canard configurations at the wings and fins for the Mach numbers of 0.6 to 2 respectively. The vector plot reveals that flow separation and reattachment is observed for all the Mach numbers. The flow gets separated near the wing tip and then later reattaches over the missile centre body.

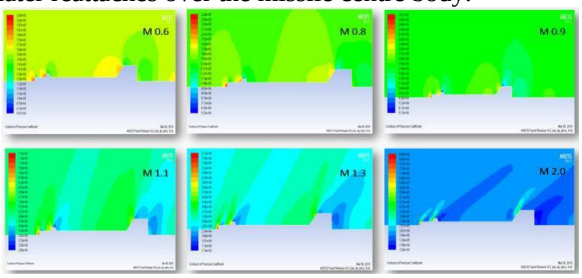

Figure 19 - Pressure contour comparison of configuration 2 for all Mach numbers

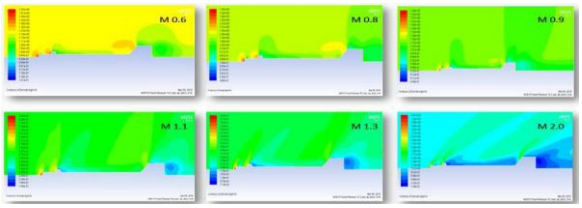

Figure 20 - Density contour comparison of configuration 2 for all Mach numbers

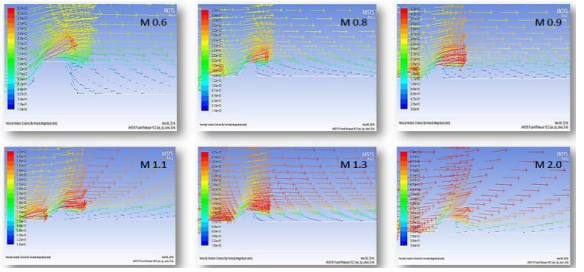

Figure 21 - Velocity vectors at wings of configuration 2 for all Mach numbers

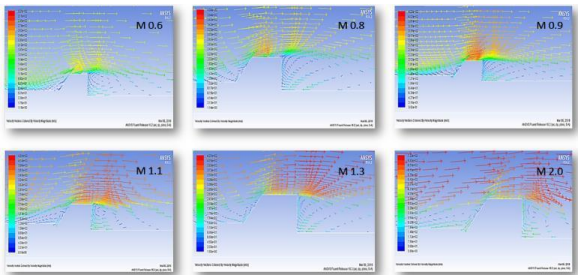

Figure 22 - Velocity vectors at fins of configuration 2 for all Mach numbers

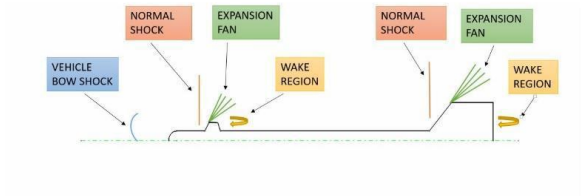

Figure 23 - The location of shock waves over Configuration 2

VI. CONCLUSION

CFD simulations have been carried out over the canard configuration for Mach numbers ranging from 0.6 to 2. The following observations are made:

1. The supersonic region seen over the canard wing and the fin is due to the occurrence of expansion fans and it is terminated by transonic shock.

2. The transonic shock observed near the canard wing and the fin moves further downstream with increase in freestream Mach number.

3. The wake region or recirculation region is observed soon after the wings and the fins.

4. The wake region increases with increase in freestream Mach numbers from 0.6 to 1.1, and then it decreases for Mach numbers 1.3 and 2.

REFERNCES

[1] A.B.Blair, Jr., jerry m. Allen, and Gloria Hernandez, "Effect of tail- fin span on stability and control charicteristics of an canard-controlled missile at supersonic mach number", Langley Research center, June 1983.

[2] Curtis P.Mracek and D. Brett Ridgely, "Optimal control solution for duel tail and canard control missile", Raytheon Missile Systems, January 2006.

[3] Hong Chuan Wee, "Aerodynamic analysis of a canard missile configuration using ANSYS-CFX", Defence Science & Technology Agency, Singapore, December 2011.

[4] James Despirito, Milton E. Vaughn Jr. & W. David, "Numerical investigation of aerodynamic of canard-controlled missile using planar and grid tail fins - subsonic and transonic flow", Weapons and Materials Research, U.S. Army Aviation and Missile Command, March 2004.

[5] Scott M. Murman, "Cartesian-grid simulations of a canard-controlled missile with a spinning tail", NASA, Ames Research Centre, June 2003.